



Article

Ni Supported on Natural Clays as a Catalyst for the Transformation of Levulinic Acid into γ -Valerolactone without the Addition of Molecular Hydrogen

Adrián García ¹, Rut Sanchis ¹, Francisco J. Llopis ¹, Isabel Vázquez ¹, María Pilar Pico ²,
María Luisa López ³, Inmaculada Álvarez-Serrano ³  and Benjamín Solsona ^{1,*} 

¹ Departament d'Enginyeria Química, ETSE, Universitat de València, Av. Universitat, Burjassot, 46100 Valencia, Spain; adrian.garcia@uv.es (A.G.); rut.sanchis@uv.es (R.S.); francisco.llopis@uv.es (F.J.L.); isabel.vazquez@uv.es (I.V.)

² Sepiolsa, Avda. del Acero, 14-16, Pol. UP-1 (Miralcampo), 19200 Azuqueca de Henares, Spain; maria.pico@sepiolsa.com

³ Departamento de Química Inorgánica, Facultad de Ciencias Químicas, Universidad Complutense de Madrid, 28040 Madrid, Spain; marisal@ucm.es (M.L.L.); ias@ucm.es (I.Á.-S.)

* Correspondence: benjamin.solsona@uv.es; Tel.: +34-963543735

Received: 11 May 2020; Accepted: 1 July 2020; Published: 3 July 2020



Abstract: γ -Valerolactone (GVL) is a valuable chemical that can be used as a clean additive for automotive fuels. This compound can be produced from biomass-derived compounds. Levulinic acid (LA) is a compound that can be obtained easily from biomass and it can be transformed into GVL by dehydration and hydrogenation using metallic catalysts. In this work, catalysts of Ni (a non-noble metal) supported on a series of natural and low-cost clay-materials have been tested in the transformation of LA into GVL. Catalysts were prepared by a modified wet impregnation method using oxalic acid trying to facilitate a suitable metal dispersion. The supports employed are attapulgite and two sepiolites with different surface areas. Reaction tests have been undertaken using an aqueous medium at moderate reaction temperatures of 120 and 180 °C. Three types of experiments were undertaken: (i) without H₂ source, (ii) using formic acid (FA) as hydrogen source and (iii) using Zn in order to transform water in hydrogen through the reaction $\text{Zn} + \text{H}_2\text{O} \rightarrow \text{ZnO} + \text{H}_2$. The best results have been obtained combining Zn (which plays a double role as a reactant for hydrogen formation and as a catalyst) and Ni/attapulgite. Yields to GVL higher than 98% have been obtained at 180 °C in the best cases. The best catalytic performance has been related to the presence of tiny Ni particles as nickel crystallites larger than 4 nm were not present in the most efficient catalysts.

Keywords: levulinic acid; γ -valerolactone; hydrogen from water; Zn; Ni; sepiolite; attapulgite

1. Introduction

Due to the gradual depletion of oil and restrictions on its use to preserve the environment and reduce climate change effects nowadays, new technologies and methods have been developed to produce fuels and valuable chemicals from renewable resources [1]. New resources have been studied to obtain these chemicals and fuels, especially biomass derivatives. Biomass is a renewable and abundant resource in Nature [2–4] with notable environmental advantages. Many products can be produced from biomass by different methods [5] such as, for example, levulinic acid (LA), which can be easily obtained from carbohydrates or lignocelluloses and it can be transformed into γ -valerolactone (GVL) by hydrogenation through different catalytic routes [6].

Interestingly, GVL has very low toxicity and presents good transport and storage properties. GVL is a colorless liquid with low melting point (−31 °C), open cup flash (96 °C) and high boiling

point (207 °C). All these characteristics make GVL an easy and safe to store chemical [7–10]. GVL can be produced cheaply and can be a useful additive to different automotive fuels, reducing undesired emissions while maintaining or barely decreasing performance. GVL can be mixed with gasoline and diesel fuels, leading to a decrease in harmful CO, residual hydrocarbon and particulate matter emissions [11,12]. For example, it has been reported that upon mixing 7% of GVL with diesel fuel the engine performance hardly varies but the smoke produced is reduced by 25% compared to the same diesel fuel without the addition of GVL [13]. Thus, GVL can help combat air pollution and mitigate global warming. In another work, GVL was recommended as a lighter fluid for charcoal and as an illuminating liquid since does not create smoke or odor, producing low levels of VOC emissions [14]. GVL also presents good properties as a green solvent [5,7] and can be a precursor for other valuable chemicals such as alkyl valerates, 4-hydroxypentanol, butanes, 2-methyltetrahydrofuran and adipic acid (nylon) [7–10,15,16].

There are different catalytic alternatives to transform LA into GVL. Thus, this catalytic reaction can be homogeneous or heterogeneous. The heterogeneous pathway is more interesting due to the easier separation of the catalyst and is usually carried out with catalysts containing noble or non-noble metals. Despite the fact non-noble metals are invariably cheaper, they have been less studied because noble metal catalysts give higher conversions at low temperatures, especially those with ruthenium [17–20]. Nevertheless, many studies have used non-noble metals to produce high added value chemicals from biomass [21–28], and nickel sites are some of the most usual active metal sites.

The use of metals deposited on inexpensive supports has been studied for the conversion of LA into GVL [29–32]. In this context, it is of interest to use clay minerals as supports because they are abundant and cheap natural materials. These supports usually present high surface areas and this can lead to a good dispersion of metals on their surface, and as a consequence, this can increase the catalytic activity compared to metals deposited on low surface area supports [33]. Therefore, we have thought that the synthesis of nickel supported on clay minerals can be an interesting option.

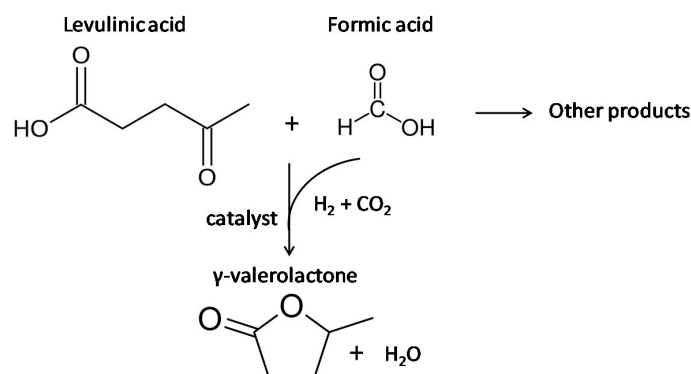
The choice of a suitable solvent is also highly important. Unfortunately, there are no solvents without any drawbacks [11,12]. Alcohols, such as isopropanol and 2-butanol, are good options with the additional advantage of promoting the catalytic transfer hydrogenation of levulinic acid into valerolactone. Hydrogen gas solubility in alcohols is slightly higher than in water, but the GVL selectivity is usually higher in water. Alcohols might assist the activation of LA for conversion, but water seems to favor the pathways for selective GVL production. In many cases alcohols are used to mitigate the leaching of metals, which is higher in aqueous media. Other solvents such as dioxane and THF have been also studied as solvents, presenting some advantages in terms of reaction temperature required or extent of metal leaching, but they are toxic and non-environmentally friendly. Overall, water can be considered as the greenest solvent from any viewpoint considered: human health, safety and environment [12].

The catalytic conversion of LA into GVL involves two steps. Firstly, LA has to be hydrogenated to produce 4-hydroxypentanoic acid as a reaction intermediate or dehydrated to form angelica lactone. In the next step the intermediates can form GVL in two possible ways: 4-hydroxypentanoic acid is cyclized and dehydrated or angelica lactone is reduced [11,34–36].

Molecular hydrogen is commonly used in the hydrogenation step [37,38], but it has problems due to its high cost and difficult storage and transport. Formic acid (FA) has been explored as a hydrogen donor, and there are studies about hydrogenation of LA into GVL using this compound with different metallic catalysts [39–41]. FA can be decomposed into H₂ and CO₂ using efficient catalysts, and this hydrogen can be used to transform LA into GVL thus avoiding the need for an external hydrogen supply (Scheme 1). The advantage of using FA for LA hydrogenation lies in the possible cost reduction. Moreover, FA can be formed together with LA when is obtained from sugars.

Another possibility to avoid the use of molecular hydrogen is through the in-situ production of hydrogen from water using metallic catalysts. This catalytic route has been explored in some studies with different non-noble metals for very different applications [42,43]. One of these catalytic routes

would involve the use of zinc (Zn) to produce hydrogen from water [44]. Zn has been used in other studies for the transformation of LA into GVL [45]. Then, Zn is able to react with water in order to produce H₂ although in parallel ZnO is also formed. The ZnO formation is, in fact, one of the main problems of using Zn, as it has to be reduced again if we want to re-use the catalyst several times. However, it is possible to reduce the ZnO into Zn in a percentage higher than 90% using solar energy [46–48]. Then, the oxidation of Zn would be less troublesome if solar energy was used to reduce the oxide for a new use [49].



Scheme 1. Reaction of hydrogenation of levulinic acid into γ -valerolactone employing formic acid as hydrogen donor.

Table 1 lists recent studies about Ni catalysts for GVL synthesis using as substrates levulinic acid or its derivatives methyl levulinate (ML) and ethyl levulinate (EL) [50–65]. In many cases, Ni was supported on different materials or mixed with other metals to increase its catalytic activity. Most of these reactions were carried out with molecular hydrogen [50,53–57,59–64], whereas other studies [28,30,51,52] used 2-propanol or formic acid as a hydrogen source [58,64].

Table 1. Overview of Ni catalysts for GVL synthesis from methyl levulinate (ML), ethyl levulinate (EL) and levulinic acid (LA).

Catalyst	Substrate	Solvent	H ₂ Source	T (°C)	Time (h)	GVL Yield (%)	Ref.
Ni-Zr-O	ML	Water	Molecular H ₂	200	3	98	[50]
				170	3	97	
				150	3	95	
Ni-Cu/SBA-15	ML	2-propanol	2-propanol	170	3	87	[30]
RANEY Ni	ML	2-propanol	2-propanol	120	1	94	[51]
RANEY Ni	EL	2-Propanol	2-propanol	80	2	99	[28]
Ni/ZrO ₂	ML	2-propanol	2-propanol	100	20	94	[52]
	LA	2-propanol	2-propanol	120	20	86	
Ru-Ni/Meso-C	LA	H ₂	Molecular H ₂	150	2	96	[53]
Ni/NiO	LA	Dioxane	Molecular H ₂	120	4,5	99	[54]
Ni/Mg ₂ Al ₂ O ₅	LA	Dioxane	Molecular H ₂	160	1	99	[55]
Ni/Al-LDH	LA	Water	Molecular H ₂	200	6	100	[56]
Ni/HZSM-5	LA	Dioxane	Molecular H ₂	220	10	93	[57]
Ni-Cu/SiO ₂	LA	N ₂	Formic acid	285	-	98	[58]
10NiNb/TiO ₂	LA	Water	Molecular H ₂	275	-	25	[59]
Cu/Ni/Mg/Al	LA	Dioxane	Molecular H ₂	140	3	100	[60]
Ni/SiO ₂	LA	H ₂	Molecular H ₂	250	0.3	89	[61]
Ni/Al ₂ O ₃	LA	H ₂	Molecular H ₂	200	4	92	[62]
Ni/HZSM-5	LA	H ₂	Molecular H ₂	320	0.5	99	[63]
Ni/SiO ₂ -Al ₂ O ₃	LA	THF	Molecular H ₂	200	0.5	100	[64]
		Isopropyl alcohol	Isopropyl alcohol		0.25	99	
		Water	Formic acid		10	70	

In this paper we have studied the use of Ni supported on different clay minerals (two different sepiolites and attapulgite) as a catalyst in the transformation of levulinic acid into γ -valerolactone. Moreover, we have compared the use of different hydrogen sources (formic acid and water as a result of its reaction with Zn) to perform the hydrogenation of LA into GVL at two different temperatures: 120 and 180 °C. The novelty of the present work is focused on two main aspects: (i) molecular hydrogen has not been used and (ii) we have used catalysts containing nickel supported on cheap and abundant materials (extracted from quarries), which have not been previously reported in this reaction.

2. Materials and Methods

2.1. Preparation of Catalysts

Ni was supported on attapulgite, which was collected from Senegal and provided by Sepiolsa (Azuqueca de Henares, Spain). The natural attapulgite used in the present work also contains some other phases, being its percentage composition the following: attapulgite 86 wt.%, smectite: 10 wt.%, quartz: 3 wt.%, dolomite: 1 wt.%. Catalysts were synthesized by a wet impregnation method using ethanol as a solvent. Different Ni concentrations were used by adding the appropriate amount of nickel nitrate ($\text{Ni}(\text{NO}_3)_2 \cdot 6\text{H}_2\text{O}$ from Sigma–Aldrich, St. Louis, MO, USA, >98%) and oxalic acid dihydrate ($\text{H}_2\text{C}_2\text{O}_4 \cdot 2\text{H}_2\text{O}$ also from Sigma–Aldrich) with a molar Ni:oxalic acid ratio of 1:3. Oxalic acid has been used in the synthesis as it is an organic acid with reducing character which is often used in these preparation procedures to decrease the crystallite size of metals and metal oxides such as in the case of nickel, this way increasing the amount of available nickel sites [66,67]. Attapulgite was added to the mixture and placed in a hotplate stirrer at 60 °C under vigorous stirring until all the solvent was evaporated. These catalysts were labeled as xNi/Atap, being x the Ni content (1, 2 and 5 wt.% were tested).

Two wt.% Ni was selected to synthesize other catalysts using different materials as supports. These supports have been named as Sep and Sep B. Both supports consist of sepiolite collected from Toledo (Spain), and also provided by Sepiolsa. The natural sepiolites used in this work present some other phases. Their composition was: sepiolite 97.0 wt.%, dolomite: 1.9 wt.%, other clays 1.1%. Both supports present the same composition but differ in their crystallinity and surface areas. Thus, the sample called “Sep” is less crystalline than “Sep B”. The surface area of “Sep” is $242 \text{ m}^2 \cdot \text{g}^{-1}$ whilst that of “Sep B” is $381 \text{ m}^2 \cdot \text{g}^{-1}$. The corresponding supported nickel catalysts were called 2Ni/Sep and 2Ni/SepB, respectively. These sepiolite-based catalysts were prepared by an impregnation method using oxalic acid, as in the case of the Ni/Atap catalysts.

Finally, samples were dried at 100 °C for 12 h and later treated at 500 °C in air for 2 h. Before the reaction and in order to reduce metal oxide precursors, catalysts were heat-treated for 2 h in a flow of H_2 at 400 °C. We decided to reduce in H_2 at 400 °C since at this temperature all the nickel is present as metallic nickel (according to our TEM results). Chemical analysis of 2Ni/Sep, 2Ni/SepB and 2Ni/Atap showed Ni loadings (2.0, 2.1 and 2.1 wt.%, respectively) very close to the theoretical values.

2.2. Characterization Techniques

Catalysts were analyzed by high resolution TEM (HR-TEM), employing a field emission gun TECNAI G2 F20 microscope (FEI Company, Hillsboro, OR, USA) at 200 kV and a JEM 3000F microscope (JEOL, Tokyo, Japan, 300 kV), in order to analyze their structure and morphology. This equipment was also used for energy dispersive X-ray (EDX) and selected area electron diffraction (SAED). Catalyst samples for TEM were sonicated for 20 min in absolute ethanol and deposited on a holey carbon film supported on a copper grid. Then, the copper grid was dried. TEM photographs were used to calculate the average size of the nickel particles. Particle-size histograms were typically constructed by measuring between 80 and 100 particles, depending on the catalyst.

X-ray diffraction (XRD) was used in order to know the crystalline phases of the catalysts and to check if nickel was oxidized or reduced. The apparatus utilized is an Enraf Nonius FR590 sealed

tube diffractometer (Bruker, Delft, The Netherlands) equipped with a monochromatic Cu K α 1 source (30 mA and 40 kV).

N₂ adsorption was undertaken at −196 °C, with a Micromeritics ASAP 2460 apparatus (Micromeritics, Norcross, GA, USA). Samples were firstly degassed at 150 °C before reaching vacuum conditions. Total pore volumes were obtained using the adsorbed volume at a relative pressure of 0.97. The specific surface area following the multipoint Brunauer–Emmet–Teller approach (S_{BET}) was obtained at the 0.05 to 0.25 relative pressure range. The pore size distribution was determined employing the Barrett–Joyner–Halenda (BJH) method through the analysis of the N₂ adsorption isotherms.

2.3. Catalytic Tests and Analyses

The catalytic tests for the transformation of LA into GVL were carried out in a 13 mL stainless steel autoclave. The inner steel walls of the autoclave are covered by a Teflon container (made in-house). For the reaction, the autoclave was fed with 3.5 mL of water, 1.24 mmol of LA and 175 mg of catalyst. Three types of reactions were conducted: (i) without any additives, (ii) with the addition of 171.6 mg of Zn and (iii) with the addition of 2.65 mmol of FA. This way the GVL production using different hydrogen sources can be compared. Controls were realized using bare sepiolite, sepiolite B, attapulgite, Zn and FA to test the conversion of LA. Before the reaction, the autoclave was purged with N₂ to minimize the metal oxidation. Later, the autoclave was sealed and introduced in a silicon bath and stirred for 2 h at 800 rpm. This stirring rate was selected in order to ensure a good mixing between the catalyst and the reactants. The reaction was realized at two different temperatures to compare the conversion: 120 and 180 °C. After 2 h, the autoclave was immediately cooled in an ice-bath to stop the reaction. Finally, the dispersion was filtered with an appropriate membrane to obtain the product in order to be analysed.

The analysis of the products has been undertaken as in [21] and [45]. GVL and LA were analyzed by gas chromatography (GC), using a mod. 5890 GC instrument (Hewlett Packard, Palo Alto, CA, USA). This GC has an Agilent HP-1 column (30 m \times 0.32 mm \times 0.25 μ m), a FID detector working at 240 °C, and an injection port at 220 °C. The temperature program for the chromatographic cycle was as follows: (i) 35 °C isothermal for 6 min, (ii) a heating rate of 20 °C min^{−1} from 35 to 230 °C and (iii) 230 °C isothermal for 26 min. Controls without LA and without catalysts were also undertaken and analysed to compare with the other reaction samples. The retention times for γ -valerolactone and levulinic acid are 5.4 and 9.5 min, respectively. Other reaction products were identified using gas chromatography-mass spectrometry (GC-MS 5977A MSD-7890A, Agilent, Santa Clara, CA, USA). The catalytic tests carried out with FA were also analyzed by GC-MS (GC-MS 5977A MSD-7890A, Agilent).

3. Results

Characterization Results

Figure 1 shows the XRD patterns of the Ni catalysts prepared on different supports before (A) and after (B) their reduction. For comparative purposes, the XRD patterns of the supports are also shown.

In the XRD pattern of pure sepiolite, all maxima have been indexed to an orthorhombic symmetry with space group Pnan [68]. Sepiolite is a silicate with fibrous characteristics presenting an ideal formula $[\text{Si}_{12}\text{Mg}_8\text{O}_{30}(\text{OH})_4](\text{H}_2\text{O})_4 \cdot 8\text{H}_2\text{O}$. It has a layered structure made up of large tunnels parallel to the phyllosilicate ribbons (Figure 2A) which are partly occupied by H₂O molecules. These tunnels measure 3.7×10.6 Å in cross section.

As it is well known, if sepiolite is heat treated structural modifications due to the loss of water molecules are observed. Preisinger [69] reported that the loss of the bound H₂O leads to a phase change during which the structure is folded by rotation of the phyllosilicate ribbons. These ribbons rotate around an axis through the Si–O–Si corner bonds which link the ribbons (Figure 2B).

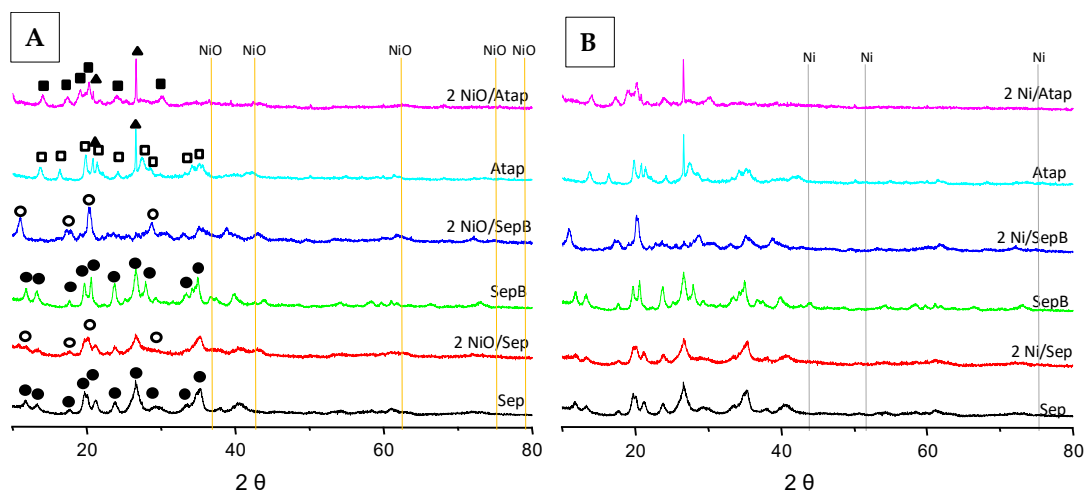


Figure 1. XRD patterns of NiO precursors (A) and final Ni catalysts (B) and the supports (Sep, SepB and Atap). Symbols: (●) sepiolite, (o) sepiolite-dehydrated, (□) attapulgite, (■) attapulgite-dehydrated, (▲) quartz. — NiO, — Ni.

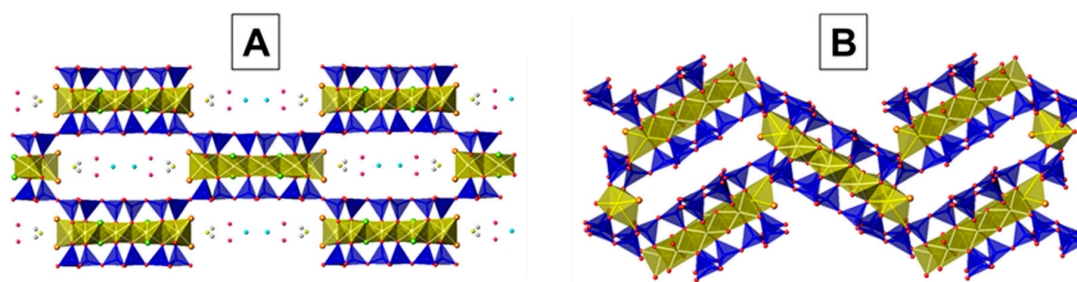


Figure 2. Schematic representation of sepiolite structure (A) before and (B) after thermal treatment.

Thus, a phase change takes place at ~ 600 – 650 K for the sepiolite heat treated in air. This transition is likely due to the folding of the sepiolite structure when the first moiety of the structural H_2O is lost. This sepiolite “anhydride” is designated as “Sepiol- $2\text{H}_2\text{O}$ ”, where “ $2\text{H}_2\text{O}$ ” corresponds to the two remaining structural molecules of H_2O .

The Bragg maxima in the XRD pattern of 2Ni/SepB have been indexed on the basis of this structure. The structural change due to the folding becomes irreversible at 570°C [70]. In this sense, the Ni/Sep catalysts seem to be formed by a mixture of Sep and Sepiol- $2\text{H}_2\text{O}$, since the thermal treatment of these phases did not exceed 500°C .

On the other hand, attapulgite exists in structurally related orthorhombic and monoclinic forms. In the XRD pattern of pure attapulgite (Figure 1), all maxima have been indexed on the basis of an orthorhombic structure. Moreover, there are two maxima that could be assigned to SiO_2 quartz, as indicated with triangles in Figure 1A. Similarly to sepiolite, attapulgite is a fibrous silicate (ideal formula $(\text{Mg}_2\text{Al}_2)(\text{Si}_8)\text{O}_{20}(\text{OH})_2(\text{H}_2\text{O})_4$) presenting a layer structure built from large tunnels parallel to the phyllosilicate ribbons which are partly occupied by H_2O molecules. These tunnels measure $3.7 \times 6 \text{ \AA}$ in cross section. In the thermal treatment in air of this clay a structural change to a folded structure also occurs. Indeed, the maxima corresponding to this folded phase, Atap-dehydrated, are observed in the XRD pattern of Ni/Atap samples (Figure 1A).

The XRD patterns of the Ni precursors (Figure 1A) show in the case of the catalysts with attapulgite and sepiolite Sep a pattern very similar to that of the pure supports whereas Sep B was affected by the calcination and a diffractogram with new peaks was observed. We should indicate that the peaks at $2\theta = 37.3^\circ$, 43.3° and 63.2° are typical of face-centered cubic crystalline structure of nickel oxide (represented by lines in the Figure 1A) and, however, these reflections have not been clearly observed in these precursors although a low intensity peak at $2\theta = 43.3^\circ$ cannot be completely ruled

out. This absence of peaks must be due to the fact that the amount of nickel is very low and NiO particles are well dispersed on the support.

In the XRD patterns of the Ni-based catalysts (Figure 1B), it can be observed that catalysts seem to be reduced as the low intensity NiO peak observed in the precursors is now absent. However, it is not possible to see the main peaks of metallic Ni ($2\theta = 44.5^\circ, 51.1^\circ, 76.1^\circ$) likely due to the low concentration of nickel in the catalysts and to the low size of nickel particles.

The textural properties of the Ni catalysts supported on different materials were determined by N_2 adsorption-desorption. BET equation was used to determine the specific surface area and the results are shown in Table 2. All the Ni catalysts displayed reduced specific surface areas compared to the support materials. The surface area of the standard sepiolite (Sep) is $242 \text{ m}^2\cdot\text{g}^{-1}$, which slightly decreases after the nickel incorporation. Then, the surface area for 2Ni/Sep is $202 \text{ m}^2\cdot\text{g}^{-1}$. The Sep B support reaches a high surface area of $381 \text{ m}^2\cdot\text{g}^{-1}$ but drastically decreases until $121 \text{ m}^2\cdot\text{g}^{-1}$ in the final Ni-catalyst. This drop is in agreement with the variations observed by XRD in which different patterns are observed in the support and in the final Ni-catalyst. Thus, after the thermal treatment which provokes a folding in the structure, the surface area of the catalysts decreases, in good agreement with the existing literature [70].

Table 2. Textural properties of the Ni-based catalyst supported on different materials.

Sample	$S_{\text{BET}} (\text{m}^2\cdot\text{g}^{-1})$	$V_T (\text{cm}^3\cdot\text{g}^{-1})$
Sep	242	0.392
2Ni/Sep	202	0.447
SepB	381	0.619
2Ni/SepB	121	0.579
Atap	216	0.499
2Ni/Atap	75	0.440

In the case of the attapulgite a notable decrease of the surface area was also observed ($216 \text{ m}^2\cdot\text{g}^{-1}$ in the support vs $75 \text{ m}^2\cdot\text{g}^{-1}$ in the final catalyst). Again, this fact could be related to the folding of the structure as a consequence of the thermal treatment, in good agreement with the XRD data, as commented above.

Figure 3A shows the isotherms patterns for the catalysts with 2 wt.% Ni supported on both sepiolites and attapulgite, and their corresponding single supports. According to the IUPAC classification the isotherms of the catalysts and the supports were classified as Type IV [71]. These isotherms patterns are typical for mesoporous adsorbents, therefore showing the mesoporous nature of the sepiolite and attapulgite clays. No big differences were appreciated between the shape of the isotherms corresponding to the supports and those for the final catalysts. However, as mentioned above there are important differences in the amount of N_2 adsorbed.

The pore distribution of the catalysts with Ni content of 2 wt.% is shown in Figure 3B. The original supports present a maximum at ca. 4 nm corresponding to the presence of small mesopores, as typical of this type of clays [72]. However, only in the Ni catalyst on the standard sepiolite (2Ni/Sep catalyst) the maximum at about 4 nm is still visible whereas it is absent in 2Ni/Atap and 2Ni/SepB. This confirms the collapse of the structures of attapulgite and the sepiolite B after the nickel incorporation and the heat-treatments. This data is in agreement with the slight decrease of the surface area in the case of Sep and the drastic drop in the catalysts with attapulgite and the Sep B.

The microstructural characteristics of the supported catalysts were analyzed by high resolution transmission electron microscopy (HRTEM). Figure 4 shows the HRTEM images and corresponding histograms of the 2Ni/Sep, 2Ni/SepB and 2Ni/Atap catalysts.

Clay-support fibers with length varying from 50 nm to several μm and widths ranging between 5 and 20 nm can be clearly observed. The analysis of the nickel-containing particles showed the presence of metal nickel and the absence of NiO particles. Periodical contrasts of 0.21 nm in the images, which

correspond to (111) interplanar distances of cubic Ni (inset of Figure 4A), indicate the crystallinity of the Ni nanoparticles. Moreover, when a magnet is placed close to the samples, the particles are attracted by the magnet. This is a typical behaviour of metallic Ni which is ferromagnetic and this would not happen if the particles were NiO, which is antiferromagnetic. Therefore, the presence of Ni nanoparticles can be undoubtedly assumed. These Ni nanoparticles are covering the clay support with similar homogeneity in all the cases and present an average size around 3 nm. In a very small extent, they appear agglomerated in clusters of 6–9 nm in size. Taking into account the particle size distribution histograms (insets in Figure 4A–C), Ni nanoparticles of an average size 3 nm are predominant in all the cases. However, whereas for 2Ni/Sep ca. 25% of the particles are larger than 4 nm, the 2Ni/SepB and 2Ni/Atap catalysts are practically composed only of nanoparticles with sizes less than 4 nm.

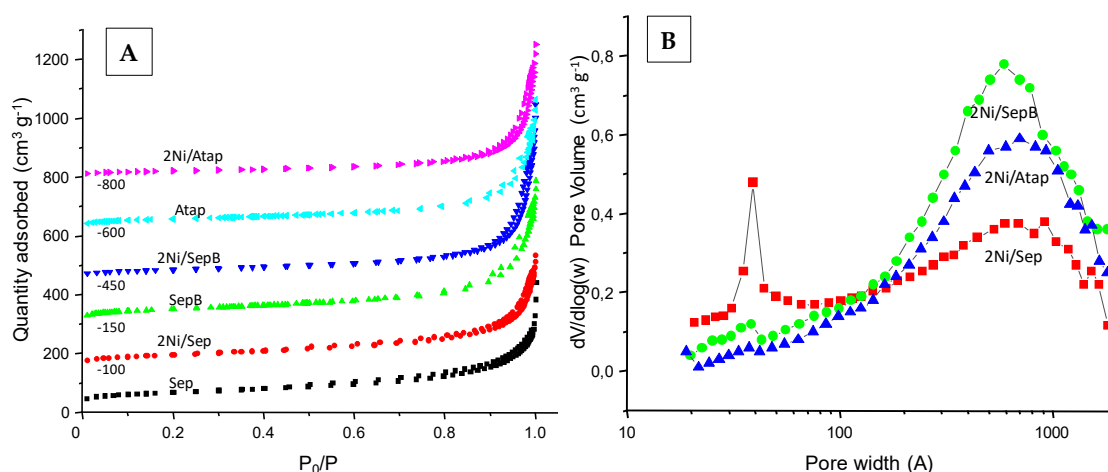


Figure 3. N₂ isotherms patterns for the catalysts with 2 wt.% Ni supported on different materials (A) and representative pore distributions (B).

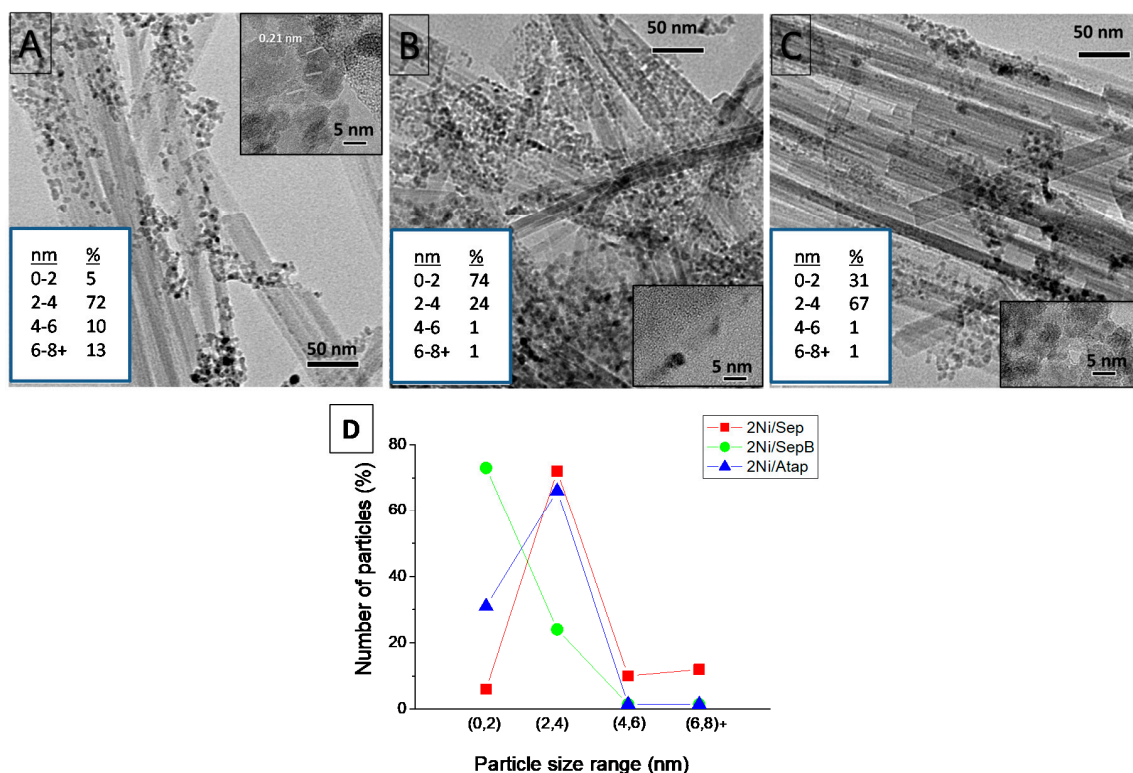


Figure 4. Representative HRTEM images for (A) 2Ni/Sep, (B) 2Ni/SepB and (C) 2Ni/Atap catalysts, and (D) distribution of the size of Ni particles in these catalysts.

Initially, different amounts of Ni (1, 2 and 5 wt.%) were supported on attapulgite in order to check the amount of nickel to use with the different supports. These Ni/attapulgite catalysts were tested in the transformation of LA at 180 °C. These preliminary tests were undertaken in the absence of formic acid or Zn. For comparison, data of an unsupported Ni catalyst prepared in the same way (catalyst named as 100Ni) is also included. Figure 5 shows that GVL was produced in all cases. GVL yield was 16% in the unsupported Ni catalyst whereas the blank experiment without catalyst gave no conversion of LA to GVL. It is noteworthy that catalysts with 2 and 5 wt.% Ni obtained yields of ca. 13%, which are very close to that achieved by the catalyst with 100% Ni. The Ni amount of 2 wt.% was selected to prepare the catalysts with the different supports because it has a similar conversion into GVL than 5 wt.%, but its productivity per Ni loading is the highest of all the catalysts tested.

This reaction has been undertaken without an external hydrogen source. However, H₂ proceeds from the water molecules as nickel reacts with water leading to the formation of metal oxide and hydrogen (according to $\text{Ni} + \text{H}_2\text{O} \rightarrow \text{NiO} + \text{H}_2$). Nickel then acts as both source of hydrogen and catalyst for the AL to GVL transformation.

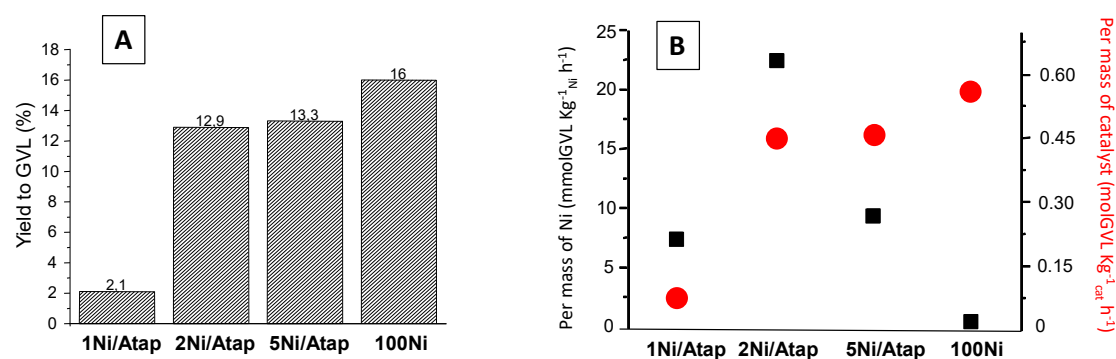


Figure 5. Influence on the Ni-loading in Ni/attapulgite catalysts (A) on the conversion of LA into GVL and (B) on the GVL productivity per mass of catalyst (●) or per mass of Ni (■). Reaction conditions: T = 180 °C, 3.5 mL of water, 1.24 mmol of LA and 175 mg of catalyst.

Then, a Ni loading of 2 wt.% was selected to be used for the impregnation of the three supports. The first assays were carried out with LA, water and in the absence of another hydrogen source. Then two different assays in the presence of either Zn or formic acid were undertaken in order to produce additional hydrogen (Zn from the reaction with water and formic acid from its decomposition). The experiments were conducted at two different reaction temperatures (120 °C and 180 °C). It must be indicated that in all cases the main reaction product observed has been γ -valerolactone with selectivities over 95%. Then, at the two tested temperatures other compounds were identified by GC-MS as byproducts of the reaction although in low amount. These compounds were 5-methyl 2(3H)-furanone and 5-methyl 2(5H)-furanone.

Table 3 shows the GVL yield and productivity results obtained by the catalysts with different hydrogen sources at 120 °C and 180 °C. The reactions carried out without hydrogen source with 2Ni/Sep, 2Ni/SepB and 2Ni/Atap show low GVL yield in all cases. At 120 °C the yields to GVL did not exceed 5.1% whereas at 180 °C the yield never reached 15%. As expected, the LA conversion and the GVL formation increase when the reaction temperature increases.

Interestingly, upon adding Zn (that plays mainly the role of reactant as mentioned above) to the nickel catalysts the catalytic activity highly increased. Then at 120 °C in all cases the LA conversion exceeded 70%, being similar with 2Ni/SepB and 2Ni/Atap, giving 82% and 82.7% of GVL yield, respectively. In the case of the 2Ni/sep catalyst the yield to GVL was lower (72.6%). The same trend was observed working at 180 °C. Using 2Ni/SepB and 2Ni/Atap catalysts all the LA reacted, leading to GVL yields higher than 98%. Lower GVL yield (85%) was obtained with 2Ni/Sep catalyst.

Using formic acid in the medium the results were very poor. Thus, the GVL yield results obtained using formic acid as hydrogen source were much worse than those achieved using Zn. In fact, lower

yields to GVL were obtained in the presence of formic acid than in its absence. Although formic acid at appropriate temperatures and with a suitable catalyst decomposes into H_2 and CO_2 , in the conditions employed in this article the dissociation of acid formic was low and did not help in the production of GVL. Thus, none of the used catalysts gave a GVL yield higher than 7% at the two different tested temperatures. It seems that the presence of formic acid hinders the hydrogen formation from water ($Ni + H_2O \rightarrow NiO + H_2$) originated by the presence of nickel. It is also possible that the negative effect of formic acid is due to the fact that metallic nickel reacts with formic acid, this leading to the formation of hydrogen, and then no active nickel sites are available to undertake the hydrogenation of levulinic acid.

Table 3. Yield of LA into GVL (%) and productivity (mmol GVL/g catalyst/h and mmol GVL/g Ni/h) using Ni on different supports and hydrogen sources.^a

Catalyst	Additional H ₂ Source	GVL Yields		molGVL kg ⁻¹ _{catalyst} h ⁻¹		molGVL kg ⁻¹ _{Ni} h ⁻¹	
		180 °C	120 °C	180 °C	120 °C	180 °C	120 °C
2 Ni/Sep	No	14.6	2.31	0.510	0.082	25.8	4.08
2 Ni/SepB	No	12.0	5.05	0.428	0.180	21.3	8.93
2 Ni/Atap	No	12.9	1.01	0.451	0.040	22.7	1.77
2 Ni/Sep	Zn added	85.2	72.6	3.01	2.57	151	128
2 Ni/SepB	Zn added	>98	82.0	3.54	2.90	177	145
2 Ni/Atap	Zn added	>98	82.7	3.54	2.92	177	146
2 Ni/Sep	Formic acid	5.39	6.50	0.187	0.233	9.52	11.5
2 Ni/SepB	Formic acid	3.02	4.54	0.111	0.156	5.41	8.02
2 Ni/Atap	Formic acid	4.02	6.26	0.142	0.219	7.09	11.1

^a Reaction conditions: water (3.5 mL), LA (1.24 mmol), 2 wt.% supported metal catalyst (175 mg) reaction temperature (180 °C and 120 °C), time (2 h) and Zn (171.6 mg) or FA (122 mg).

Comparing these three strategies, the use of Zn turns out to be the most effective in transforming LA into GV. Thus, the productivity to GVL is at least one order of magnitude higher when using Zn than when using formic acid or without using additives. Analyses of the gas of the batches demonstrates that in all the experiments done with the Ni-catalysts some hydrogen was formed, being much more abundant in the experiments with Zn. The quantification of the hydrogen has not been possible to be carried out with high accuracy due to experimental limitations.

For comparison a 2 wt.% Ni catalyst supported on silica (Aerosil, surface area 181 m²·g⁻¹) was prepared in the same way and tested in the LA transformation in the presence of Zn at 180 °C. It was observed that this option also produced high amounts of GVL (yield = 73.7%) but less than comparable catalysts with natural clays as supports. Controls were undertaken in the three conditions mentioned above but in the absence of catalyst. Then, with formic acid or without additives the levulinic acid conversion was negligible. However, in the case of using Zn alone a yield to GVL of 35% was obtained at 180 °C. Then in the experiments undertaken with Ni/catalysts and Zn at 180 °C the catalytic role of both Zn and nickel sites must be considered in order to explain the catalytic performance. In these control experiments hydrogen was detected in the gas-phase in the test using Zn in contrast with the experiment in which additives were not added.

4. Discussion

Ni is an effective non-noble metal capable of producing the conversion of LA into GVL with high efficiency. This way, the use of noble metals is avoided making this process less expensive. In fact, we have observed that it is possible to produce GVL in high yield using small amounts of Ni supported on cheap and highly available supports employing an easy preparation method by impregnation with oxalic acid. The best results have been obtained with 2Ni/SepB and 2Ni/Atap using Zn as a hydrogen source.

In the Ni catalysts supported on clays, nanoparticles cover the support with similar homogeneity and with most particles presenting a size of ca. 3 nm. However, on attapulgite or on the more crystalline sepiolite (Sep B) there are no nickel particles larger than 4 nm, whereas on the standard sepiolite there is an important portion of big particles of 6–9 nm in size. This microstructural feature is probably connected to the better performance of the 2Ni/SepB and 2Ni/Atap catalysts compared to 2Ni/Sep. Then, the higher GVL yields obtained with nickel on attapulgite or on Sep B is likely linked to the lower presence of big nickel particles than on the standard sepiolite. Then, for a fixed nickel loading (2.0–2.1 wt.% in our catalysts) the lower the crystallite size the higher the amount of available active sites is. We want to mention that the catalytic role of the environment around Ni sites cannot be neglected, although the similitude between the support surfaces, lead us to conclude that the main differences are likely due to the different nickel crystallite size. Similarly, in [73,74] it was shown that Ni sites can catalyze hydrogen transfer reactions through a coupling effect, and dispersed Ni nanoparticles present the highest catalytic efficiency in the LA to GVL reaction whereas bare Ni foam could not activate LA. Interestingly, the solvent has a crucial role in the hydrogen transfer reaction because could interact with the metal and react to supply hydrogen.

In order to confirm that metallic Zn had been oxidized to ZnO, samples of Ni-catalysts with Zn were collected after reaction at 120 °C and 180 °C and they were analyzed by XRD. Figure 6A shows the XRD patterns of the 2Ni/sepB catalyst with Zn after reaction at 120 °C and 180 °C. In the sample used at 120 °C, apart from the diffractions of the Ni-catalyst, high intensity peaks corresponding to ZnO (JCPDS: 36-1451) were observed. However, diffractions of metallic Zn (JCPDS: 04-0831) were hardly observed. Then, at 120 °C more than 95% of the initial metallic Zn has been transformed into ZnO in the presence of water with the consequent hydrogen formation. In the sample used at 180 °C, apart from diffractions of ZnO (main crystalline phase detected) and Zn, peaks corresponding to a new Zn-containing phase are observed at $2\theta = 12.7, 21.7, 22.1, 25.5, 31.5, 34.0, 38.8$ and 49.0° (only cited the most intense). This pattern fits well with that of a Zn-silicate (Zn_2SiO_4 phase, JCPDS: 08-0492). Then, in this case Zn/ZnO reacts with part of the silicon of the sepiolite to form this new phase.

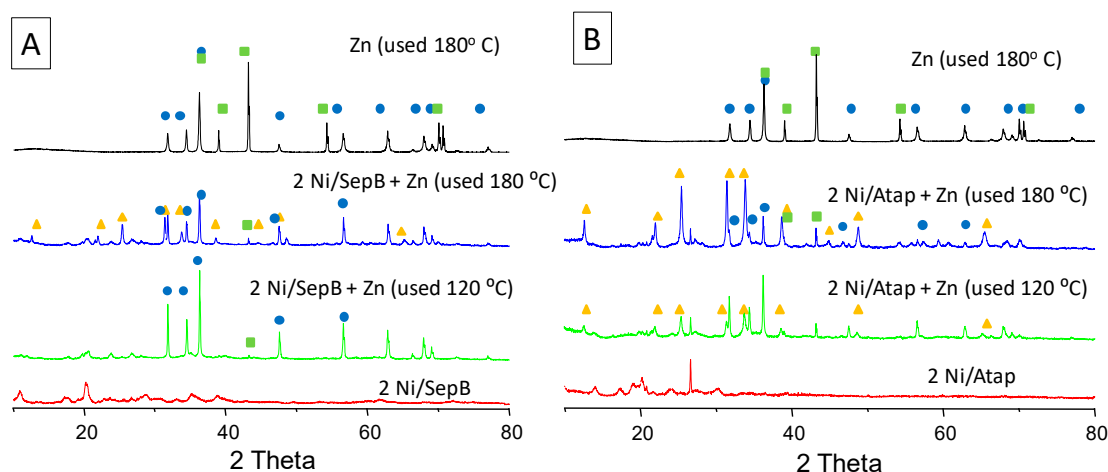


Figure 6. XRD patterns of 2Ni/SepB (A) and 2Ni/Atap (B): fresh, after use at 120 °C with Zn and after use at 180 °C with Zn. For comparison the XRD pattern of Zn used at 180 °C has been also included. Symbols: (■) Zn^0 , (●) ZnO, (▲) Zn_2SiO_4 .

Figure 6B shows the XRD patterns of the 2Ni/Atap catalyst with Zn after reaction at 120 °C and 180 °C. In the experiment undertaken at 120 °C apart from the diffractions of the Ni-catalyst, intense peaks of ZnO were detected. The relative intensity of the most intense peaks of ZnO compared to Zn is ca. 5, which is lower than that observed with 2Ni/SepB, in which almost all of the zinc was present as ZnO. Moreover, in this sample the formation of Zn_2SiO_4 phase is already visible at 120 °C in contrast with 2Ni/SepB. This fact could be explained taking into account the presence of some amount

of quartz as a secondary phase in the pristine attapulgite, as observed by XRD data and commented above (Figure 1A). In the sample at 180 °C the main reflections correspond to Zn_2SiO_4 phase whereas peaks of lower intensity of Zn and ZnO have also been detected. These results indicate that silicon from attapulgite reacts with Zn/ZnO to form the Zn-silicate phase.

The XRD pattern of the Zn alone sample used at 180 °C shows that ca. 40% of Zn is oxidized into ZnO. This oxidation takes place to a lesser extent than when zinc is together with Ni/SepB or Ni/Atap catalysts (Table 4). It seems that the presence of the nickel catalysts initially accelerates the Zn oxidation to ZnO and then, especially at high temperatures, reacts with a part of the support.

Table 4. Relative intensity of the most intense XRD peaks of Zn, ZnO and Zn_2SiO_4 in used samples.

Experiment/Sample	Reaction Temperature (°C)	ZnO/Zn	$\text{Zn}_2\text{SiO}_4/\text{Zn}$
Zn alone	180	0.71	-
2Ni/SepB + Zn	120	98	0
2Ni/SepB + Zn	180	8.9	4.0
2Ni/Atap + Zn	120	5.2	2.2
2Ni/Atap + Zn	180	1.5	3.5

A microscopy study of the Zn + 2Ni/SepB sample used at 120 °C shows sepiolite fibers with small patches of nickel together with large particles of ZnO (Figure 7). As indicated above, the length of the sepiolite fibers ranges from 50–100 nm to 4 µm whereas their width varies from 5 to 20 nm. The particles of ZnO are quite heterogeneous in size and shape although most of them are rectangular with typical length of 200–300 nm and width of 80–150 nm. In the initial microscopy study, it was observed that nickel of the fresh Ni/supported catalysts was present as metallic nickel. In Figure 7c we can observe by HRTEM a particle containing nickel deposited on a sepiolite rod. The lighter part of the particle likely corresponds to nickel oxide ($d_{\text{hkl}} = 0.21$ and 0.24 nm, assigned to NiO 200 and NiO 111, respectively) whilst the darkest part probably corresponds to metallic nickel ($d_{\text{hkl}} = 0.20$ and 0.18 nm assigned to Ni 111 and Ni 200, respectively). Then, after the reaction not only is Zn oxidized but also a part of the metallic nickel transforms into NiO. It must be mentioned that the size of Ni/NiO particles in the used catalyst was similar to that of the fresh catalyst and, overall, no enlargement of the particles is apparent. Nevertheless, although most of particles (>95%) were smaller than 6 nm, a couple of large particles (>15 nm) were also observed in the used sample.

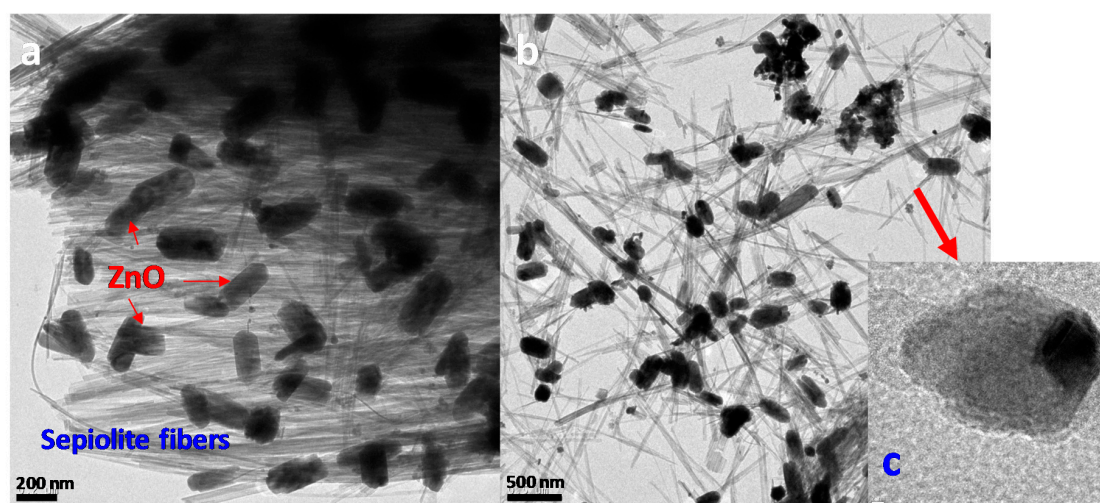


Figure 7. TEM (a,b) and HRTEM (c) images of 2Ni/Sep B with Zn after use at 120 °C.

The reaction using 2Ni/Atap and adding Zn was selected to study the influence of the reaction time in the GVL yield. Two more catalytic tests were carried out for 1 and 6 h at 120 °C (Figure 8).

After 1 h of reaction the yield to GVL was 53.6% and after 2 h the yield to GVL had increased to 82.7%. However, for longer reaction times (6 h) the yield to GVL (84.3%) remained almost identical to that after 2 h. This scarce increase must be due to the fact that after 2 h most of the Zn is already transformed into ZnO (Figure 8B) and then from 2 to 6 h there is hardly any hydrogen available for further reaction. In order to corroborate this, Figure 8B shows the XRD patterns of 2Ni/Atap with Zn after 1, 2 and 6 h of reaction at 120 °C. It can be observed that when the reaction time increases metallic Zn is transformed into ZnO and Zn₂SiO₄. Then, after 1 h there is a high amount of Zn available whereas after 2 h it has drastically decreased. Finally, after 6 h there is not any metallic Zn.

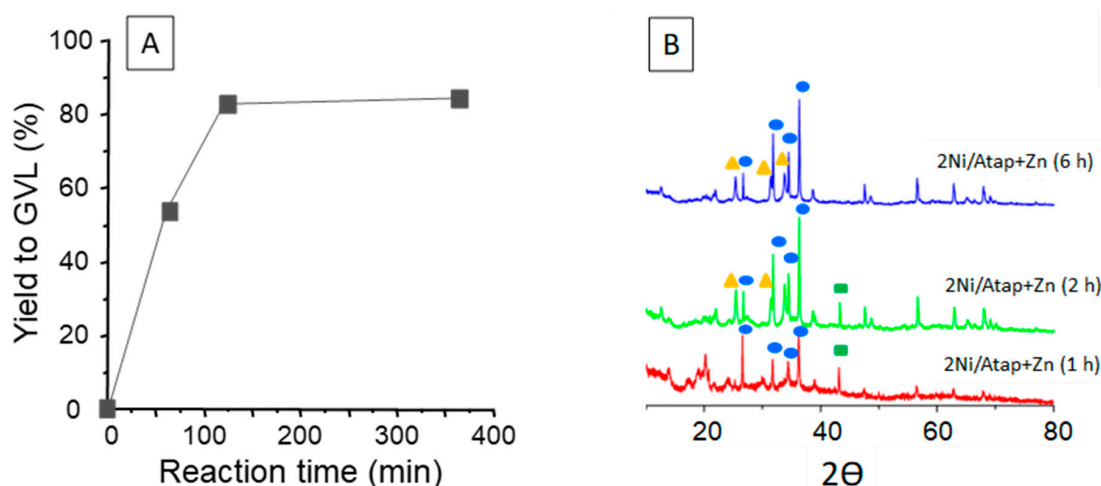


Figure 8. Effect of the reaction time on the yield to GVL (■) using 2Ni/Atap + Zn at 120 °C (A) with their corresponding XRD after use (B). Symbols: (■) Zn⁰, (●) ZnO, (▲) Zn₂SiO₄.

Finally, the recyclability of 2Ni/Atap was studied. After use under standard conditions at 120 °C, the mixture of Ni/Atap + Zn was collected and dried. Then a further catalytic experiment, with a previous reduction, was conducted at 120 °C under standard conditions. Before the second test we had Zn not yet oxidized during the reaction plus metallic Zn obtained from the reduction of the ZnO of the sample used in the first test. As a part of the used mixture could not be collected we assume that the loss of Ni/Atap and Zn is proportional. Then, in the re-testing experiment it was observed a moderate drop in the GVL productivity per mass of catalyst from 2.92 mol GVL kg^{−1}_{catalyst} h^{−1} in the fresh catalyst to 2.29 mol GVL kg^{−1}_{catalyst} h^{−1} in the re-used catalyst. This drop of the productivity could be related to: (i) the formation of the Zn-silicate after use which could modify both the nature of the catalytic sites and the amount of the hydrogen available from the oxidation of Zn and (ii) to the leaching of the nickel active sites. In fact, it can be observed by microscopy that the used catalyst has lower density of nickel nanoparticles than the fresh catalyst. A third re-testing led to a moderate drop in the productivity (2.22 mol GVL kg^{−1}_{catalyst} h^{−1}).

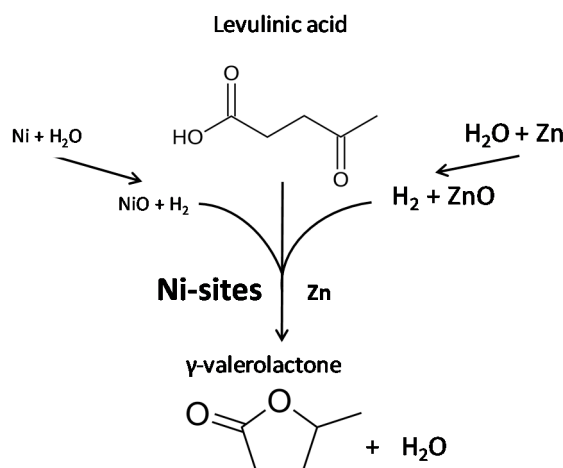
We must indicate that a similar recyclability test at 120 °C but without previous reduction led to a drastic drop of the GVL productivity (from 2.92 mol GVL kg^{−1}_{catalyst} h^{−1} in the fresh catalyst to 0.42 mol GVL kg^{−1}_{catalyst} h^{−1} in the re-used catalyst) probably due to the low hydrogen availability in the reaction medium and maybe to the lack of activation ability of the oxidized nickel.

One of the positive aspects of this catalytic system is the low loss of catalytic activity after use if there is a previous reduction. However, there is a lack of structural stability as during the catalytic reaction the supports react with Zn forming a new phase (Zn-silicates). Interestingly, in spite of this lack of structural stability a drastic deterioration of the catalytic performance has not been observed.

The presence of both metals (Ni and Zn) is essential because Ni is able to transform LA into GVL in the presence of hydrogen and Zn is able to produce hydrogen when it reacts with water. In purity, both nickel sites and Zn can play both roles: (i) produce hydrogen from water and (ii) be catalytically active in the dehydration/hydrogenation of LA to GVL. However, attending to the catalytic results

obtained the main role of Zn sites is the supply of hydrogen from its reaction with water whereas the main role of nickel sites is catalytic (hydrogenation/dehydration) (Scheme 2).

Finally, we would like to indicate that the use of metals to produce hydrogen through the reaction with water presents the drawback of the need of a further reduction to be re-used. However, the use of other options such as propanol or formic acid requires new feedings of these compounds, as they are spent during reaction. Therefore, a possible advantage of the approach followed in the present article is that, if the catalytic system is stable enough, it would not be necessary to add fresh metals for the new cycles.



Scheme 2. Reaction of hydrogenation of levulinic acid into γ -valerolactone using the reaction of Zn with water to produce H₂ and Ni/sepiolite catalysts.

Overall, the results presented in this article are notorious since GVL yields greater than 98% have been obtained at 180 °C and these are among the best catalytic results reported using other options without feeding molecular hydrogen (Table 1). Now, the next objective is to achieve a further improvement in the stability of the system so that it could be reused without worsening the catalytic performance.

5. Conclusions

Ni-catalysts supported on inexpensive and readily available supports (sepiolites with different crystallinity and attapulgite) were tested in the transformation of levulinic acid into γ -valerolactone in an aqueous medium using three different alternatives without added pressurized H₂: (i) no hydrogen source, (ii) adding Zn to the reaction mixture and (iii) adding formic acid. The reactions carried out without any hydrogen source or using formic acid led to low γ -valerolactone yields. The use of Ni supported on attapulgite or on a high surface area sepiolite has led to yields to γ -valerolactone higher than 98% using Zn in the reaction media at 180 °C. Moreover, the structure folding of the clays after thermal treatment seems to provide best yield to GVL. The best performance of nickel on attapulgite or on high surface area sepiolite is likely related to the lower size of nickel particles on these two supports compared to low surface area sepiolite, leading to a higher amount of available active sites. During these experiments, Zn transforms into ZnO and also reacts with the silicon of the supports to form Zn₂SiO₄, this limiting their reusability. Interestingly, the catalytic performance of the mixture of the Ni-catalyst + Zn can be restored to a large extent.

Author Contributions: Conceptualization, B.S.; methodology, R.S.; formal analysis, F.J.L.; investigation, A.G., R.S., I.Á.-S.; resources, M.P.P., M.L.L.; data curation, A.G., I.V.; writing—original draft preparation, A.G.; writing—review and editing, B.S., F.J.L., I.V.; visualization, F.J.L., I.V.; supervision, B.S.; project administration, M.L.L., I.Á.-S.; funding acquisition, B.S., M.P.P., M.L.L., I.Á.-S. All authors have read and agreed to the published version of the manuscript.

Funding: Authors from UCM thank MINECO (MAT2017-84118-C2-2-R project) and UCM CAI center of EM. Authors from UV thank MINECO (MAT2017-84118-C2-1-R project) an FEDER for funding. A.G. thanks MINECO for the pre-doctoral grant.

Acknowledgments: SCSIE from UV is also acknowledged for characterization of the materials employed and the GC-MS analyses. Said Agouram is acknowledged for assistance in the microscopy experiments. Miranda Sánchez is acknowledged for assistance in the catalytic work.

Conflicts of Interest: The authors declare no conflict of interest.

References

1. Mika, L.; Cséfalvay, E.; Németh, Á. Catalytic conversion of carbohydrates to initial platform chemicals: Chemistry and sustainability. *Renew. Sustain. Energy Rev.* **2017**, *118*, 505–613. [\[CrossRef\]](#)
2. Escobar, J.; Lora, E.; Venturini, O.; Yáñez, E.; Castillo, E.; Almazan, O. Biofuels: Environment, technology and food security. *Renew. Sustain. Energy Rev.* **2009**, *13*, 1275–1287. [\[CrossRef\]](#)
3. Serrano-Ruiz, J.; Sepulveda-Escribano, A. Transformations of biomass-derived platform molecules: From high added-value chemicals to fuels via aqueous-phase processing. *Chem. Soc. Rev.* **2011**, *43*, 5266–5281. [\[CrossRef\]](#) [\[PubMed\]](#)
4. Deng, L.; Li, J.; Lai, D.; Fu, Y.; Guo, Q. Catalytic conversion of biomass-derived carbohydrates into γ -valerolactone without using an external H_2 supply. *Angew. Chem. Int. Ed.* **2009**, *121*, 6651–6654. [\[CrossRef\]](#)
5. Alonso, D.; Wettstein, S.; Dumesic, J. Gamma-valerolactone, a sustainable platform molecule derived from lignocellulosic biomass. *Green Chem.* **2013**, *15*, 584–595. [\[CrossRef\]](#)
6. Orłowski, I.; Douthwaite, M.; Iqbal, S.; Hayward, J.; Davies, T.; Bartley, J.; Miedziak, P.; Hirayama, J.; Morgan, D.; Willock, D.; et al. The hydrogenation of levulinic acid to γ -valerolactone over Cu–ZrO₂ catalysts prepared by a pH-gradient methodology. *J. Energy Chem.* **2019**, *36*, 15–24. [\[CrossRef\]](#)
7. Gelosia, M.; Ingles, D.; Pompili, E.; D’Antonio, S.; Cavalaglio, G.; Petrozzi, A.; Coccia, V. Fractionation of Lignocellulosic Residues Coupling Steam Explosion and Organosolv Treatments Using Green Solvent γ -Valerolactone. *Energies* **2017**, *10*, 1264. [\[CrossRef\]](#)
8. Qi, L.; Horváth, I. Catalytic conversion of fructose to γ -valerolactone in γ -valerolactone. *ACS Catal.* **2012**, *2*, 2247–2249. [\[CrossRef\]](#)
9. Zhang, Z. Synthesis of γ -valerolactone from carbohydrates and its applications. *Chem. Sus. Chem.* **2016**, *9*, 156–171. [\[CrossRef\]](#)
10. Horváth, I.; Mehdi, H.; Fábos, V.; Boda, L.; Mika, L. γ -Valerolactone—a sustainable liquid for energy and carbon-based chemicals. *Green Chem.* **2008**, *10*, 238–242. [\[CrossRef\]](#)
11. Dutta, S.; Yu, I.K.M.; Tsang, D.C.W.; Ng, Y.H.; Ok, Y.S.; Sherwood, J.; Clark, J.H. Green synthesis of gamma-valerolactone (GVL) through hydrogenation of biomass-derived levulinic acid using non-noble metal catalysts: A critical review. *Chem. Eng. J.* **2019**, *372*, 992–1006. [\[CrossRef\]](#)
12. Prat, D.; Wells, A.; Sneddon, H.; McElroy, C.R.; Abou-Shehadeh, S.; Dunn, P.J. CHEM21 selection guide of classical and less classical solvents. *Green Chem.* **2016**, *18*, 288–296. [\[CrossRef\]](#)
13. Bereczky, A.; Lukács, K.; Farkas, M.; Dóbbé, S. Effect of γ -Valerolactone Blending on Engine Performance, Combustion Characteristics and Exhaust Emissions in a Diesel Engine. *Nat. Resour.* **2014**, *5*, 177–191.
14. Fábos, V.; Lui, M.Y.; Mui, Y.F.; Wong, Y.Y.; Mika, L.T.; Qi, L.; Cséfalvay, E.; Kovács, V.; Szűcs, T.; Horváth, I.T. Use of Gamma-Valerolactone as an Illuminating Liquid and Lighter Fluid. *ACS Sustain. Chem. Eng.* **2015**, *3*, 1899–1904. [\[CrossRef\]](#)
15. Tuck, C.O.; Pérez, E.; Horváth, I.T.; Sheldon, R.A.; Poliakoff, M. Valorization of Biomass: Deriving More Value from Waste. *Science* **2012**, *337*, 695–699. [\[CrossRef\]](#)
16. Lange, J.P.; Price, R.; Ayoub, P.M.; Louis, J.; Petrus, L.; Clarke, L.; Gosselink, H. Valeric biofuels: A platform of cellulosic transportation fuels. *Angew. Chem. Int. Edit.* **2010**, *49*, 4479–4483. [\[CrossRef\]](#)
17. Ruppert, A.M.; Agulhon, P.; Grams, J.; Wachała, M.; Wojciechowska, J.; Świerczyński, D.; Cacciaguerra, T.; Tanchoux, N.; Quignard, F. Synthesis of TiO₂–ZrO₂ Mixed Oxides via the Alginate Route: Application in the Ru Catalytic Hydrogenation of Levulinic Acid to Gamma-Valerolactone. *Energies* **2019**, *12*, 4706. [\[CrossRef\]](#)
18. Zhao, D.; Wang, Y.; Delbecq, F.; Len, C. Continuous flow conversion of alkyl levulinates into γ -valerolactone in the presence of Ru/C as catalyst. *Mol. Catal.* **2019**, *475*, 110456. [\[CrossRef\]](#)

19. Van Nguyen, C.; Matsagar, B.; Yeh, J.; Chiang, W.; Wu, K. MIL-53-NH₂-derived carbon-Al₂O₃ composites supported Ru catalyst for effective hydrogenation of levulinic acid to γ -valerolactone under ambient conditions. *Mol. Catal.* **2019**, *475*, 110478. [[CrossRef](#)]
20. Xiao, C.; Goh, T.; Qi, Z.; Goes, S.; Brashler, K.; Perez, C.; Huang, W. Conversion of levulinic acid to γ -valerolactone over few-layer graphene-supported ruthenium catalysts. *ACS Catal.* **2015**, *6*, 593–599. [[CrossRef](#)]
21. Sanchis, R.; García, T.; Dejoz, A.; Vázquez, I.; Llopis, F.; Solsona, B. Easy method for the transformation of levulinic acid into gamma-valerolactone using a nickel catalyst derived from nanocasted nickel oxide. *Materials* **2019**, *12*, 2918. [[CrossRef](#)] [[PubMed](#)]
22. Li, J.; Li, M.; Zhang, C.; Liu, C.; Yang, R.; Dong, W. Construction of mesoporous Cu/ZrO₂-Al₂O₃ as a ternary catalyst for efficient synthesis of γ -valerolactone from levulinic acid at low temperature. *J. Catal.* **2020**, *381*, 163–174. [[CrossRef](#)]
23. Xie, Z.; Chen, B.; Wu, H.; Liu, M.; Liu, H.; Zhang, J.; Yang, G.; Han, B. Highly efficient hydrogenation of levulinic acid into 2-methyltetrahydrofuran over Ni-Cu/Al₂O₃-ZrO₂ bifunctional catalysts. *Green Chem.* **2019**, *21*, 606–613. [[CrossRef](#)]
24. Xu, Q.; Li, X.; Pan, T.; Yu, C.; Deng, J.; Guo, Q.; Fu, Y. Supported copper catalysts for highly efficient hydrogenation of biomass-derived levulinic acid and γ -valerolactone. *Green Chem.* **2016**, *18*, 1287–1294. [[CrossRef](#)]
25. Yuan, J.; Li, S.; Yu, L.; Liu, Y.; Cao, Y.; He, H.; Fan, K. Copper-based catalysts for the efficient conversion of carbohydrate biomass into γ -valerolactone in the absence of externally added hydrogen. *Energy Environ. Sci.* **2013**, *6*, 3308–3313. [[CrossRef](#)]
26. Tanwongwan, W.; Eiad-ua, A.; Kraithong, W.; Viriya-empikul, N.; Suttisintong, K.; Klamchuen, A.; Kasamechonchung, P.; Khemthong, P.; Faungnawakij, K.; Kuboon, S. Simultaneous activation of copper mixed metal oxide catalysts in alcohols for gamma-valerolactone production from methyl levulinate. *Appl. Catal. A Gen.* **2019**, *579*, 91–98. [[CrossRef](#)]
27. Yang, Z.; Huang, Y.; Guo, Q.; Fu, Y. RANEY @Ni catalyzed transfer hydrogenation of levulinate esters to γ -valerolactone at room temperature. *Chem. Commun.* **2013**, *49*, 5328–5330. [[CrossRef](#)] [[PubMed](#)]
28. Murugesan, K.; Alshammari, A.; Sohail, M.; Jagadeesh, R. Levulinic acid derived reusable cobalt-nanoparticles-catalyzed sustainable synthesis of γ -valerolactone. *ACS Sustain. Chem. Eng.* **2019**, *7*, 14756–14764. [[CrossRef](#)]
29. Fang, C.; Kuboon, S.; Khemthong, P.; Butburee, T.; Chakthranont, P.; Itthibenchapong, V.; Kasamechonchung, P.; Wittoon, T.; Faungnawakij, K. Highly dispersed Ni Cu nanoparticles on SBA-15 for selective hydrogenation of methyl levulinate to γ -valerolactone. *Int. J. Hydrog. Energ.* **2019**, *3*, 272–283. [[CrossRef](#)]
30. Li, C.; Ni, X.; Di, X.; Liang, C. Aqueous phase hydrogenation of levulinic acid to γ -valerolactone on supported Ru catalysts prepared by microwave-assisted thermolytic method. *J. Fuel Chem. Technol.* **2018**, *46*, 161–170. [[CrossRef](#)]
31. Li, J.; Zhao, L.; Li, J.; Li, M.; Liu, C.; Yang, R.; Dong, W. Highly selective synthesis of γ -valerolactone from levulinic acid at mild conditions catalyzed by boron oxide doped Cu/ZrO₂ catalysts. *Appl. Catal. A Gen.* **2019**, *587*, 117244. [[CrossRef](#)]
32. Jones, D.; Iqbal, S.; Ishikawa, S.; Reece, C.; Thomas, L.; Miedziak, P.; Morgan, D.; Edwards, J.; Bartley, J.; Willock, D.; et al. The conversion of levulinic acid into γ -valerolactone using Cu-ZrO₂ catalysts. *Catal. Sci. Technol.* **2016**, *6*, 6022. [[CrossRef](#)]
33. Guerrero-Torres, A.; Jiménez-Gómez, C.; Cecilia, J.; García-Sancho, C.; Franco, F.; Quirante-Sánchez, J.; Maireles-Torres, P. Ni supported on sepiolite catalysts for the hydrogenation of furfural to value-added chemicals: Influence of the synthesis method on the catalytic performance. *Top. Catal.* **2019**, *62*, 535–550. [[CrossRef](#)]
34. Jing, Y.; Guo, Y.; Xia, Q.; Liu, X.; Wang, Y. Catalytic production of value-added chemicals and liquid fuels from lignocellulosic biomass. *Chemicals* **2019**, *5*, 2520–2546. [[CrossRef](#)]
35. Upare, P.; Lee, J.; Hwang, D.; Halligudi, S.; Hwang, Y.; Chang, J. Selective hydrogenation of levulinic acid to γ -valerolactone over carbon-supported noble metal catalysts. *J. Ind. Eng. Chem.* **2011**, *17*, 287–292. [[CrossRef](#)]
36. Putrakumar, B.; Nagaraju, N.; Kumar, V.; Chary, K. Hydrogenation of levulinic acid to γ -valerolactone over copper catalysts supported on γ -Al₂O₃. *Catal. Today* **2015**, *250*, 209–217. [[CrossRef](#)]

37. Manzer, L. Catalytic synthesis of α -methylene- γ -valerolactone: A biomass-derived acrylic monomer. *Appl. Catal. A Gen.* **2004**, *272*, 249–256. [\[CrossRef\]](#)
38. Lange, J.; Vestering, J.; Haan, R. Towards 'bio-based' nylon: Conversion of γ -valerolactone to methyl pentenoate under catalytic distillation conditions. *Chem. Commun.* **2007**, *33*, 3488–3490. [\[CrossRef\]](#)
39. Feng, J.; Gu, X.; Xue, Y.; Han, Y.; Lu, X. Production of γ -valerolactone from levulinic acid over a Ru/C catalyst using formic acid as the sole hydrogen source. *Sci. Total Environ.* **2018**, *633*, 426–432. [\[CrossRef\]](#)
40. Du, X.; He, L.; Zhao, S.; Liu, Y.; Cao, Y.; He, H.; Fan, K. Hydrogen-independent reductive transformation of carbohydrate biomass into γ -valerolactone and pyrrolidone derivatives with supported gold catalysts. *Angew. Chem. Int. Ed.* **2011**, *50*, 7815–7819. [\[CrossRef\]](#)
41. Son, P.; Nishimura, S.; Ebitani, K. Production of γ -valerolactone from biomass-derived compounds using formic acid as a hydrogen source over supported metal catalysts in water solvent. *Rsc Adv.* **2014**, *4*, 10525–10530. [\[CrossRef\]](#)
42. Damma, D.; Smirniotis, P. Recent advances in iron-based high-temperature water-gas shift catalysis for hydrogen production. *Curr. Opin. Chem. Eng.* **2018**, *21*, 103–110. [\[CrossRef\]](#)
43. Mastuli, M.; Kamarulzaman, N.; Kasim, M.; Sivasangar, S.; Saiman, M.; Taufiq-Yap, Y. Catalytic gasification of oil palm frond biomass in supercritical water using MgO supported Ni, Cu and Zn oxides as catalysts for hydrogen production. *Int. J. Hydrogen Energy* **2017**, *42*, 11215–11228. [\[CrossRef\]](#)
44. Jin, F.; Zeng, X.; Liu, J.; Jin, Y.; Wang, L.; Zhong, H.; Yao, G.; Huo, Z. Highly efficient and autocatalytic H_2O dissociation for CO_2 reduction into formic acid with zinc. *Sci. Rep.* **2015**, *4*, 1–8. [\[CrossRef\]](#)
45. Zhong, H.; Li, Q.; Liu, J.; Yao, G.; Wang, J.; Zeng, X.; Huo, Z.; Jin, F. New method for highly efficient conversion of biomass-derived levulinic acid to γ -valerolactone in water without precious metal catalysts. *ACS Sustain. Chem. Eng.* **2017**, *5*, 6517–6523. [\[CrossRef\]](#)
46. Steinfeld, A.; Brack, M.; Meier, A.; Weidenkaff, A.; Wüillemin, D. A solar chemical reactor for co-production of zinc and synthesis gas. *Energy* **1998**, *23*, 803–814. [\[CrossRef\]](#)
47. Osinga, T.; Olalde, G.; Steinfeld, A. Solar carbothermal reduction of ZnO: Shrinking packed-bed reactor modeling and experimental validation. *Ind. Eng. Chem. Res.* **2004**, *43*, 7981–7988. [\[CrossRef\]](#)
48. Haueter, P.; Moeller, S.; Palumbo, R.; Steinfeld, A. The production of zinc by thermal dissociation of zinc oxide—Solar chemical reactor design. *J. Sol. Energy.* **1999**, *67*, 161–167. [\[CrossRef\]](#)
49. Yadav, D.; Banerjee, R. A comparative life cycle energy and carbon emission analysis of the solar carbothermal and hydrometallurgy routes for zinc production. *Appl. Energy.* **2018**, *229*, 577–602. [\[CrossRef\]](#)
50. Sun, M.; Xia, J.; Wang, H.; Liu, X.; Xia, Q.; Wang, Y. An efficient Ni_xZr_yO catalyst for hydrogenation of bio-derived methyl levulinate to γ -valerolactone in water under low hydrogen pressure. *Appl. Catal. B Environ.* **2018**, *227*, 488–498. [\[CrossRef\]](#)
51. Geboers, J.; Wang, X.; de Carvalho, A.B.; Rinaldi, R. Densification of biorefinery schemes by H-transfer with Raney Ni and 2-propanol: A case study of a potential avenue for valorization of alkyl levulinates to alkyl γ -hydroxypentanoates and γ -valerolactone. *J. Mol. Catal. A Chem.* **2014**, *388–389*, 106–115. [\[CrossRef\]](#)
52. Sakakibara, K.; Endo, K.; Osawa, T. Facile synthesis of γ -valerolactone by transfer hydrogenation of methyl levulinate and levulinic acid over Ni/ZrO₂. *Catal. Commun.* **2019**, *125*, 52–55. [\[CrossRef\]](#)
53. Yang, Y.; Gao, G.; Zhang, X.; Li, F. Facile Fabrication of Composition-Tuned Ru–Ni Bimetallics in Ordered Mesoporous Carbon for Levulinic Acid Hydrogenation. *ACS Catal.* **2014**, *4*, 1419–1425. [\[CrossRef\]](#)
54. Song, S.; Yao, S.; Cao, J.; Di, L.; Wu, G.; Guan, N.; Li, L. Heterostructured Ni/NiO composite as a robust catalyst for the hydrogenation of levulinic acid to γ -valerolactone. *Appl. Catal. B Environ.* **2017**, *217*, 115–124. [\[CrossRef\]](#)
55. Jiang, K.; Sheng, D.; Zhang, Z.; Fu, J.; Hou, Z.; Lu, X. Hydrogenation of levulinic acid to γ -valerolactone in dioxane over mixed MgO–Al₂O₃ supported Ni catalyst. *Catal. Today.* **2016**, *274*, 55–59. [\[CrossRef\]](#)
56. Gundekari, S.; Srinivasan, K. In situ generated Ni(0)@boehmite from NiAl-LDH: An efficient catalyst for selective hydrogenation of biomass derived levulinic acid to γ -valerolactone. *Catal. Commun.* **2017**, *102*, 40–43. [\[CrossRef\]](#)
57. Yi, Z.; Hu, D.; Xu, H.; Wu, Z.; Zhang, M.; Yan, K. Metal regulating the highly selective synthesis of gamma-valerolactone and valeric biofuels from biomass-derived levulinic acid. *Fuel* **2020**, *259*, 116208. [\[CrossRef\]](#)

58. Upare, P.P.; Jeong, M.; Hwang, Y.K.; Kim, D.H.; Kim, Y.D.; Hwang, D.W.; Lee, U.-H.; Chang, J. Nickel-promoted copper-silica nanocomposite catalysts for hydrogenation of levulinic acid to lactones using formic acid as a hydrogen feeder. *Appl. Catal. A Gen.* **2015**, *491*, 127–135. [\[CrossRef\]](#)
59. Peddakasu, G.B.; Velisoju, V.K.; Kandula, M.; Gutta, N.; VR Chary, K.; Akula, V. Role of group V elements on the hydrogenation activity of Ni/TiO₂ catalyst for the vapour phase conversion of levulinic acid to γ -valerolactone. *Catal. Today* **2019**, *325*, 68–72. [\[CrossRef\]](#)
60. Gupta, S.S.R.; Kantam, M.L. Selective hydrogenation of levulinic acid into γ -valerolactone over Cu/Ni hydrotalcite-derived catalyst. *Catal. Today* **2018**, *309*, 189–194. [\[CrossRef\]](#)
61. Sun, D.; Ohkubo, A.; Asami, K.; Katori, T.; Yamada, Y.; Sato, S. Vapor-phase hydrogenation of levulinic acid and methyl levulinate to γ -valerolactone over non-noble metal-based catalysts. *Mol. Catal.* **2017**, *437*, 105–113. [\[CrossRef\]](#)
62. Hengst, K.; Schubert, M.; Carvalho, H.W.P.; Lu, C.; Kleist, W.; Grunwaldt, J. Synthesis of γ -valerolactone by hydrogenation of levulinic acid over supported nickel catalysts. *Appl. Catal. A Gen.* **2015**, *502*, 18–26. [\[CrossRef\]](#)
63. Popova, M.; Djinović, P.; Ristić, A.; Lazarova, H.; Dražić, G.; Pintar, A.; Balu, A.M.; Novak Tušar, N. Vapor-Phase Hydrogenation of Levulinic Acid to γ -Valerolactone Over Bi-Functional Ni/HZSM-5 Catalyst. *Front. Chem.* **2018**, *6*, 285. [\[CrossRef\]](#) [\[PubMed\]](#)
64. Gundekari, S.; Gundekari, S.; Srinivasan, K.; Srinivasan, K. Screening of Solvents, Hydrogen Source, and Investigation of Reaction Mechanism for the Hydrocyclisation of Levulinic Acid to γ -Valerolactone Using Ni/SiO₂-Al₂O₃ Catalyst. *Catal. Lett.* **2019**, *149*, 215–227. [\[CrossRef\]](#)
65. Yu, Z.; Lu, X.; Liu, C.; Han, Y.; Ji, N. Synthesis of γ -valerolactone from different biomass-derived feedstocks: Recent advances on reaction mechanisms and catalytic systems. *Renew. Sustain. Energy Rev.* **2019**, *112*, 140–157. [\[CrossRef\]](#)
66. Solsona, B.; López Nieto, J.M.; Agouram, S.; Soriano, M.D.; Dejoz, A.; Vázquez, M.I.; Concepción, P. Optimizing Both Catalyst Preparation and Catalytic Behaviour for the Oxidative Dehydrogenation of Ethane of Ni-Sn-O Catalysts. *Top. Catal.* **2016**, *59*, 1564–1572. [\[CrossRef\]](#)
67. Solsona, B.; Concepción, P.; Demicol, B.; Hernández, S.; Delgado, J.J.; Calvino, J.J.; López Nieto, J.M. Selective oxidative dehydrogenation of ethane over SnO₂-promoted NiO catalysts. *J. Catal.* **2012**, *295*, 104–114. [\[CrossRef\]](#)
68. Post, J.E.; Bish, D.L.; Heaney, P.J. Synchrotron powder X-ray diffraction study of the structure and dehydration behavior of sepiolite. *Am. Mineral.* **2007**, *92*, 91–97. [\[CrossRef\]](#)
69. Preisinger, A.A. Sepiolite and related compounds: Its stability and application. *Clays Clay Miner.* **1961**, *10*, 365–371. [\[CrossRef\]](#)
70. Ruiz, R.; Del Moral, J.C.; Pesquera, C.; Benito, I.; González, F. Reversible folding in sepiolite: Study by thermal and textural analysis. *Thermochim. Acta* **1996**, *279*, 103–110. [\[CrossRef\]](#)
71. Thommes, M.; Kaneko, K.; Neimark, A.V.; Olivier, J.P.; Rodríguez-Reinoso, F.; Rouquerol, J.; Sing, K.S.W. Physisorption of gases, with special reference to the evaluation of surface area and pore size distribution (IUPAC Technical Report). *Pure Appl. Chem.* **2015**, *87*, 1051–1069. [\[CrossRef\]](#)
72. Tang, Q.; Wang, F.; Tang, M.; Liang, J.; Ren, C. Study on pore distribution and formation rule of sepiolite mineral nanomaterials. *J. Nanomater.* **2012**, *2012*, 382603. [\[CrossRef\]](#)
73. Yan, K.; Liu, Y.; Lu, Y.; Chai, J.; Sun, L. Catalytic application of layered double hydroxide-derived catalysts for the conversion of biomass-derived molecules. *Catal. Sci. Technol.* **2017**, *7*, 1622–1645. [\[CrossRef\]](#)
74. Li, W.; Fan, G.; Yang, L.; Li, F. Highly Efficient Vapor-Phase Hydrogenation of Biomass-Derived Levulinic Acid Over Structured Nanowall-Like Nickel-Based Catalyst. *Chem. Cat. Chem.* **2016**, *8*, 2724–2733. [\[CrossRef\]](#)

